Progress in Organic Coatings 189 (2024) 108246

Contents lists available at ScienceDirect

Progress in Organic Coatings

journal homepage: www.elsevier.com/locate/porgcoat

Antimicrobial chitosan/TPP-based coatings for the prevention of biodeterioration of outdoor stone sculptures

Nádia C. Silva [a], Diana Castro [a], Cláudia Neto [a], Ana Raquel Madureira [a], Manuela Pintado [a], Patrícia R. Moreira [a,b,*]

[a] Universidade Católica Portuguesa, CBQF - Centro de Biotecnologia e Química Fina – Laboratório Associado, Escola Superior de Biotecnologia, Rua Diogo Botelho 1327, 4169-005 Porto, Portugal

[b] Universidade Católica Portuguesa, CITAR - Centro de Investigação em Ciência e Tecnologia das Artes, Escola das Artes, Rua Diogo Botelho 1327, 4169-005 Porto, Portugal

ARTICLE INFO

Keywords:
Chitosan
Coating
Stone
Sculpture
Cultural heritage

ABSTRACT

Outdoor stone sculptures are prone to accelerated deterioration caused by the proliferation of microorganisms in the stone. The physical, chemical and mechanical action of microorganisms on stone heritage causes aesthetic and structural changes that devalue the artworks over time. Developing more sustainable and ecological alternatives for their preventive conservation is necessary to reduce the negative environmental and human health impacts of currently used toxic biocides. Chitosan-based coatings cross-linked with citric acid and sodium tripolyphosphate (TPP) were developed for application to stone sculptures, as antimicrobial protection to inhibit the growth of degrading microorganisms. After polymerisation of the formulations, the resulting films were only partially soluble while remaining permeable to water vapour. These characteristics offer the possibility to reverse the conservation treatments, or to re-treat in regular periods, as part of programmed conservation strategies. Bacteria and fungi commonly found in stone microbiomes that contribute to biodeterioration processes were inhibited, particularly the pigment-producing yeast *Rhodotorula* spp., which causes discolouration of stone surfaces. The most interesting coating was successfully tested on granite, limestone and marble samples, and its presence on the stones' surfaces was confirmed by FTIR and SEM analyses. The chitosan-based coating caused no visible colour changes to the stones and reduced the wettability of granite and limestone, thus representing a potential antimicrobial protective layer for stone cultural heritage.

1. Introduction

Cultural heritage, in its various forms, represents the history, identity and legacy of human societies [1,2]. The protection and conservation of cultural heritage is, therefore, a global responsibility in today's world, and its proper management must be ensured by various means, including scientific and biotechnological contributions [3–5]. In particular, tangible immovable heritage (historical and archaeological sites, monuments, buildings, sculptures, etc.) is often at risk of deterioration in a constantly changing world, and its conservation is essential to ensure that its historical, artistic and economic value is preserved and passed on to future generations [1,2,6,7]. Stone heritage, such as sculptures, is susceptible to various forms of deterioration, especially when they are placed outdoors. Urban outdoor stone sculptures are subject to the deteriorating effects of exposure to uncontrollable environmental conditions and atmospheric pollution [8–10]. Furthermore, stone degradation is exacerbated by the physical and chemical action of microorganisms that colonise the artworks (biodeterioration), promoting several aesthetic and structural changes that reduce the integrity and value of the objects over time [11,12]. Even though biodeterioration processes of outdoor sculptures cannot be fully stopped, they can be slowed down with a combination of prevention, control and intervention actions [5,10,13]. Whenever possible, biodeterioration processes should be addressed from a preventive perspective, by implementing programmed conservation strategies and protective treatments that will hinder or slow down microbial growth [14,15]. Current conservation

* Corresponding author at: Universidade Católica Portuguesa, CITAR - Centro de Investigação em Ciência e Tecnologia das Artes, Escola das Artes, Rua Diogo Botelho 1327, 4169-005 Porto, Portugal.

E-mail addresses: s-nscsilva@ucp.pt (N.C. Silva), s-dmgcastro@ucp.pt (D. Castro), rmadureira@ucp.pt (A.R. Madureira), mpintado@ucp.pt (M. Pintado), prmoreira@ucp.pt (P.R. Moreira).

https://doi.org/10.1016/j.porgcoat.2024.108246
Received 15 August 2023; Received in revised form 31 December 2023; Accepted 10 January 2024

practices using chemical compounds involve biocides and synthetic polymer coatings that can react with the substrates and have negative impacts on the artworks, such as discolouration of the materials and oxidation/reduction reactions [15,16]. They also pose environmental problems and can be toxic to human health [17].

One of the challenges in the cultural heritage conservation field today is the development of new products that constitute an alternative to traditional treatments while fulfilling a set of relevant characteristics. In particular, new solutions must be environmentally friendly, have low cost, derive from renewable sources, be easily applicable, be compatible and well absorbed by the treated surfaces, allow water vapour exchanges, not damage nor alter the structural characteristics of the materials to be preserved and not change the colour and aesthetic appearance of the artworks [11,18–21]. The reversibility of the treatments, or at least their retreatability, is also a fundamental feature in conservation practices [19,21–23]. Coatings used in preventive conservation strategies often have limited durability in terms of their effectiveness and need to be reapplied or substituted by other treatments without bringing unexpected consequences [24]. Biodegradable polymers have been considered in recent years as part of conservation treatments, since they are expected to disintegrate completely over time and leave no residues in the stone, allowing reapplications to be carried out when required, or alternative conservation treatments to be undertaken, without compromising future works due to polymer build-up [24,25].

Chitosan has many properties that have attracted interest from a variety of fields [26–31]. It is a natural biodegradable polymer derived from the deacetylation of chitin and can be obtained from shellfish waste, as chitin is part of the exoskeleton of crustaceans [29,32,33]. Chitosan's non-toxicity and proven wide range of antimicrobial activity have been explored to develop films and coatings for various applications, such as wound dressings and food packaging [29,34,35]. However, the use of chitosan in art conservation remains scarce, despite its fulfilling many of the requirements to address problems in the field, such as those related to the biodeterioration of stone cultural heritage.

In this context, we have developed chitosan formulations cross-linked with citric acid and sodium tripolyphosphate (TPP) for application to stone sculptures and artworks, as an antimicrobial protective coating to inhibit the growth of degrading microorganisms. The coating-forming solutions were evaporated to form solid films, which were characterised by Fourier Transform Infrared (FTIR) spectroscopy and evaluated for their solubility and swelling in water, wettability, water vapour transmission and antimicrobial activity against bacteria and fungi chosen among those that commonly colonise stone sculptures. The most suitable formulation was selected and applied in liquid form to samples of granite, limestone and marble. The characterisation of the coated stones was carried out by FTIR, scanning electron microscopy (SEM), wettability tests and colourimetric measurements in order to evaluate the applicability of the coating and its impact on the aesthetic properties of the different types of stone.

2. Materials and methods

2.1. Materials

Chitosan (medium molecular weight grade (190,000–310,000 Da), 75–85 % deacetylated), citric acid monohydrate, TPP, calcium chloride, peptone and TWEEN® 80 were purchased from Sigma-Aldrich (USA). Glacial acetic acid and glycerol were obtained from Merck (Germany). Potato dextrose agar (PDA) and Müller-Hinton (MH) broth and agar culture media were purchased from BIOKAR Diagnostics (France). Potato dextrose broth (PDB) was obtained from Laboratorios Conda (Spain). Granite, marble and limestone slabs were purchased from Mármores e Granitos Felisberto, Lda (Portugal).

2.2. Preparation of CHGCA-TPP formulations

The preparation of the CHGCA-TPP formulations was adapted from [36,37] with modifications. Chitosan (1 % (*w/v*)) was dissolved in an aqueous solution of 1 % (*v*/v) acetic acid to prepare the coatings. After complete dissolution, glycerol and citric acid at 1 % (w/v) were added to the chitosan solution and the resulting mixture was stirred at 600 rpm for 2 h. TPP solutions (6 mL) were prepared at 0.25 %, 0.50 % and 0.75 % (w/v) in deionised water and added dropwise to 15 mL of the previous mixture, at a flow rate of 250 μL min^{-1} (KDS 100 Legacy, KD Scientific, USA) under constant stirring (1000 rpm), in order to obtain three formulations with increasing TPP concentrations (CHGCA-TPP-a, CHGCA-TPP-b, CHGCA-TPP-c; see Table 1). The final coating-forming solutions were stirred for a further 10 min at 1000 rpm to ensure complete homogenisation.

To characterise the formulations, the coating-forming solutions were poured into plastic Petri dishes (6 mL in 52 mm diameter dishes or 16 mL in 85 mm diameter dishes) and allowed to dry at room temperature for 72 h until polymerisation into thin solid films occurred. Additionally, the coating-forming solution with the lowest TPP concentration (CHGCA-TPP-a) was applied to the upper surfaces of granite, marble and limestone slabs (previously washed and cleaned with deionised water; 400 μL in 4 × 4 × 1 cm or 25 μL in 1 × 1 × 1 cm stone slabs), spread with micropipette tips and left at room temperature for 4 h until complete drying before further analysis.

2.3. Characterisation of CHGCA-TPP formulations

2.3.1. FTIR spectroscopy

FTIR analysis of the CHGCA-TPP solid films was performed using a FTIR spectrometer (PerkinElmer Precisely Spectrum 100, Waltham, USA) equipped with an attenuated total reflectance (ATR) accessory (PIKE MIRacle™, PIKE Technologies, USA) with a diamond crystal plate. FTIR spectra were acquired with eight scans and 4 cm^{-1} resolution in the 4000–550 cm^{-1} region. Chitosan films containing only glycerol (CHG) and glycerol and citric acid (CHGCA) were also analysed and used as controls to examine the structural alterations on chitosan films due to cross-linking.

2.3.2. Evaluation of film solubility and swelling in water

The percentages of solubility and swelling of the CHGCA-TPP films were determined according to Al-Naamani et al., 2016 [38] with slight modifications. The films were dried to constant weight in an oven at 105 °C on glass Petri dishes, which had been dried and weighed beforehand under the same conditions. The initial dry weight of the films (M_1) was calculated and the films were immersed in 35 mL of deionised water. After 24 h, the water was removed, and the films were dried with filter paper to absorb excess water and weighed to calculate their wet weight (M_2) for the swelling assays. For the solubility experiments, after removing the water, the films were again placed in an oven at 105 °C for

Table 1
Chitosan and TPP mass ratios in the CHGCA-TPP formulations, thickness of the films after polymerisation and percentage of *Penicillium chrysogenum* growth inhibition after incubation with the films.

Sample	Mass (mg)		Chitosan: TPP mass ratio	Thickness (mm)	*Penicillium chrysogenum* growth inhibition (%)
	Chitosan	TPP			
CHGCA-TPP-a	146.48	14.65	5:0.5	0.040 ± 0.001[a]	21.48 ± 8.41[a]
CHGCA-TPP-b	146.48	29.30	5:1	0.046 ± 0.007[a]	12.61 ± 7.08[a]
CHGCA-TPP-c	146.48	43.94	5:1.5	0.069 ± 0.004[b]	11.92 ± 6.31[a]

24 h and weighed to obtain their final dry weight (M_3). The assays were performed in triplicate and the measurements were made using an analytical balance (ACJ 120-4M, Kern & Sohn, Germany). The swelling and solubility of the films were calculated using Eqs. (1) and (2):

$$\text{Swelling}\ (\%) = \left(\frac{M_2 - M_1}{M_1}\right) \times 100 \quad (1)$$

$$\text{Solubility}\ (\%) = \left(\frac{M_1 - M_3}{M_1}\right) \times 100 \quad (2)$$

2.3.3. Water contact angle (WCA) assessment

The WCAs of the CHGCA-TPP films were determined by the sessile drop technique (Laplace-Young method) using a tensiometer (Attension Theta, Biolin Scientific, Sweden). Each film was measured at three different points, by dispensing 3 μL of deionised water on the films and measuring the angles formed between the baseline and the tangent lines to the surfaces of the water droplets. The experiment was made in triplicate and the values were recorded for 1 min; the values after 3 s of stabilisation of the water droplets were used to calculate the mean WCA for each film.

2.3.4. Thickness and water vapour transmission rate (WVTR) assays

Thickness measurements were taken at four different points on each CHGCA-TPP film using a micrometre (MI20, Adamel Lhomargy, France). The films were measured in triplicate and the values were averaged to obtain the mean thickness.

The WVTR assays were performed by the gravimetric method. The CHGCA-TPP films were placed on aluminium cups containing anhydrous calcium chloride as a desiccant, which were covered with ring-shaped lids and sealed with paraffin and screws to hold the films to the edges of the cups. CHGCA-TPP films placed and sealed on aluminium cups without calcium chloride were used as negative controls. The cups were maintained in a room with controlled atmosphere at 22 ± 2 °C and 48 ± 4 % relative humidity and weighed over 4 days, using an analytical balance (XS205 DualRange, Mettler Toledo, Switzerland), in order to determine the amount of water vapour absorbed by calcium chloride through the membranes. The assays were performed in triplicate and the WVTRs were calculated using Eq. (3):

$$\text{WVTR}\ \left(\text{g m}^{-2}\ \text{day}\right) = \left(\frac{\text{sF} - \text{sC}}{\text{A}}\right) \times 24 \quad (3)$$

where sF is the slope of the regression lines of the weight versus time plots of the films, sC is the slope of the regression lines of the weight versus time plots of the negative controls and A is the effective area of the films.

2.3.5. Antimicrobial activity protocol

2.3.5.1. Microorganisms. The microorganisms tested were *Pseudomonas aeruginosa* (ATCC® 27853™), *Staphylococcus aureus* (ATCC® 25923™), *Bacillus cereus* (NCTC 2599), *Rhodotorula* spp. (CBS 10577) and *Penicillium chrysogenum* (ATCC® 10106™). These microorganisms were selected as representative strains of taxa that are prevalent and widespread in stone microbiomes and can cause changes in stone cultural heritage [39–42], and constitute an initial basis for evaluating the antimicrobial capacity of the chitosan formulations. The microbial cultures were maintained in MH broth (*P. aeruginosa*, *S. aureus* and *B. cereus*) or PDB (*Rhodotorula* spp. and *P. chrysogenum)* until antimicrobial activity testing.

2.3.5.2. Calibration curves. The bacterial strains were grown on MH agar at 37 °C (*P. aeruginosa* and *S. aureus*) and 30 °C (*B. cereus*) for 16 h, while the fungal cultures were grown on PDA at 22 °C for 65 h (*Rhodotorula* spp.) and at 25 °C for 4 days (*P. chrysogenum*). Cell suspensions of *S. aureus*, *B. cereus*, *P. aeruginosa* and *Rhodotorula* spp. were prepared in peptone water (1 g L^{-1}) from the respective inoculated agar plates. A solution of 1 % (*w/v*) of TWEEN® 80 in 1 g L^{-1} peptone water was used in order to extract *P. chrysogenum* spores from the PDA plates inoculated with the fungus, which were collected in a sterile tube. The cell and spore suspensions were diluted with peptone water (1 g L^{-1}) to an optical density (OD) of 0.9–1.0 at 600 nm using a spectrophotometer (UV mini-1240, Shimadzu, Japan). The suspensions were further diluted (1:2) in peptone water (1 g L^{-1}) and the OD values were recorded. Serial dilutions of 1:10 in peptone water (1 g L^{-1}) were then made from each of the diluted suspensions and 100 μL were plated in duplicate on MH agar (for the bacteria) or PDA (for the fungi) using the spread plate technique. The agar plates were incubated for 24 h (at 37 °C for *P. aeruginosa* and *S. aureus* and at 30 °C for *B. cereus*), 65 h at 22 °C for *Rhodotorula* spp. and 48 h at 25 °C for *P. chrysogenum*. The concentration of viable cells or spores was calculated according to Eq. (4):

$$\text{Concentration of viable cells or spores}\ \left(\text{CFU or spores ml}^{-1}\right) = \\ = \text{number of CFU or spores} \times \frac{1}{\text{dilution}} \times \frac{1}{\text{plated volume}} \quad (4)$$

where CFU is the number of colony-forming units.

Calibration curves of CFU mL^{-1} or spores mL^{-1} versus OD values were plotted and used to calculate the concentrations required for the viable cell count and spore concentration assays.

2.3.5.3. Viable cell count assays. Viable cell count assays were performed according to Campos et al., 2014 [43] with minor modifications. CHGCA-TPP films (in triplicate) were cut into 1 cm^2 discs, sterilised under UV-C light for 10 min on each side and placed in sterile 24-well microplates. Cell suspensions of *P. aeruginosa*, *S. aureus* and *B. cereus* were prepared in MH broth and incubated for 16 h at the temperature required for each strain, while *Rhodotorula* spp. suspensions were obtained after inoculation in PDB and incubation at 22 °C for 65 h. Each inoculum was prepared by diluting the suspensions of the corresponding microorganism in peptone water (1 g L^{-1}) to a concentration of 5×10^6 CFU mL^{-1}, as calculated from the calibration curves and the OD measurements obtained by spectrophotometry. The microplate wells containing the film discs were filled with 200 μL of inoculum and 200 μL of MH broth or PDB to completely cover the discs. Positive controls were performed under the same conditions in wells without film discs. Negative controls were performed by adding 400 μL of culture media to wells containing film discs. The microplates were incubated at 37 °C, 30 °C or 22 °C, depending on the microorganism being tested. At specific time points (0 h, 3 h, 6 h and 24 h for the bacteria; 0 h, 3 h, 6 h, 24 h, 48 h, 55 h and 78 h for the yeast), aliquots of 200 μL were aseptically taken from each well, homogenised in 1.8 mL of peptone water (1 g L^{-1}) and serially diluted (1:10) in peptone water (1 g L^{-1}). Each dilution was plated (20 μL) in triplicate on MH agar (for the bacteria) or PDA (for the yeast) by the drop plate technique and incubated for 24 h or 65 h at the temperature required for each microorganism. The concentration of viable cells was calculated according to Eq. (4). The inhibitory effect on microbial growth was estimated as the logarithmic (log) reduction in viable cells after incubation of the microorganisms with the films (Eq. (5)):

$$\text{Logarithmic growth reduction} = log_{10}\left(\frac{\text{CFU mL}^{-1}\ \text{at initial time point}}{\text{CFU mL}^{-1}\ \text{at final time point}}\right) \quad (5)$$

where CFU is the number of colony-forming units.

2.3.5.4. Spore concentration assays. The antifungal activity of the CHGCA-TPP films was evaluated by testing the ability of *P. chrysogenum* spores to germinate on the surfaces of the films, following a protocol adapted from [44,45]. A suspension of *P. chrysogenum* spores was

prepared as described in Section 2.3.5.2 and adjusted to a concentration of 2.5×10^6 spores mL^{-1} after measuring the OD in a spectrophotometer (UV mini-1240, Shimadzu, Japan) and calculating the spore concentration using the previously determined calibration curve. The films, cut into 1 cm^2 discs, were sterilised under UV-C light for 10 min on each side. The film discs were placed in the centre of PDA plates and 10 μL of the *P. chrysogenum* spore suspension was added to each film. The assays were performed in triplicate. Positive controls were prepared similarly, with the same inocula, but using sterile filter paper discs instead of film discs. Negative controls were performed by placing film discs in PDA plates without spore suspensions. The agar plates were incubated at 25 °C for 4 days and the diameter of the fungal colonies was measured to calculate the percentage of inhibition of fungal growth (Eq. (6)):

$$\text{Fungal growth inhibition } (\%) = 100 - \left(\frac{dF \times 100}{dC}\right) \quad (6)$$

where dF is the diameter of *P. chrysogenum* colonies grown on the film discs and dC is the diameter of *P. chrysogenum* colonies grown on the filter paper discs.

2.4. Characterisation of CHGCA-TPP-a-coated stone samples

2.4.1. FTIR spectroscopy

Granite, marble and limestone samples (4 × 4 × 1 cm) were coated with CHGCA-TPP-a coating-forming solution as described in Section 2.2 and the corresponding FTIR spectra were obtained as reported in Section 2.3.1. FTIR spectra of uncoated stone samples were also collected for comparison purposes.

2.4.2. SEM

Granite, marble and limestone samples (1 × 1 × 1 cm) were coated with CHGCA-TPP-a solution as described in Section 2.2. The samples were then observed under a scanning electron microscope (JEOL JSM 5600LV, Japan) in low vacuum at an accelerating voltage of 30 kV. SEM images of uncoated samples were also acquired for comparison purposes.

2.4.3. WCA measurements

The WCAs of granite, marble and limestone samples (4 × 4 × 1 cm) coated with CHGCA-TPP-a solution (see Section 2.2) were determined by applying 3 μL of deionised water to three different points on each slab using the same equipment and in the same manner as detailed in Section 2.3.3. Uncoated granite, marble and limestone were used as controls and their WCAs were also acquired. The experiment was performed in triplicate using three slabs of each stone type.

2.4.4. Colourimetry

The L* a* b* coordinates of the CIELab colour space were recorded using a CM-700d Chroma Meter (Konica Minolta, Japan), with an 8 mm aperture. Twenty measurements were taken over the entire upper surfaces of uncoated granite, marble and limestone (4 × 4 × 1 cm), and the mean values of L*, a* and b* were calculated for each sample. The same stones were coated with 400 μL of CHGCA-TPP-a solution using either a micropipette tip (as described in Section 2.2) or a brush to spread the liquid, and new colourimetric measurements were taken after 24 h. The experiment was performed in triplicate and the total colour difference (ΔE^*_{ab}) between the samples before and after coating was calculated according to Eq. (7):

$$\Delta E^*_{ab} = \left[(\Delta L^*)^2 + (\Delta a^*)^2 + (\Delta b^*)^2\right]^{1/2} \quad (7)$$

where ΔL*, Δa* and Δb* are the differences between the L*, a* and b* values of the samples before and after coating, respectively.

2.5. Statistical analysis

Statistical analysis was performed using IBM SPSS® Statistics v28 software (IBM, USA). The Shapiro-Wilk test was used to verify the normal distribution condition of the data, and one-way analysis of variance (ANOVA) with the Tukey B post-hoc test was executed to calculate significant differences among the three CHGCA-TPP formulations for the different parameters studied. For non-normally distributed data, the analysis was conducted with the Kruskal-Wallis test followed by Mann-Whitney tests. Differences in WCA values between uncoated and coated stone samples were verified by independent samples *t*-tests, as was the comparison of fungal growth inhibition values between the films and the control. Likewise, the colour differences of the stones coated with CHGCA-TPP-a using either a micropipette or a brush were analysed by independent samples t-tests.

3. Results and discussion

3.1. Physicochemical properties of CHGCA-TPP formulations

The chitosan formulations had pH values of 3–4 and their physicochemical properties were investigated after casting the coating-forming solutions into Petri dishes and polymerisation into solid films (Supplementary Fig. S1). Thin homogeneous CHGCA-TPP films were obtained (Fig. 1), which were easily recovered from the Petri dishes. The films retained their structure when immersed in water for 24 h, upon visual inspection.

3.1.1. FTIR spectroscopy

The structural changes of the chitosan films and the establishment of new chemical bonds due to the cross-linking of chitosan with citric acid and TPP were investigated by FTIR. The FTIR spectrum of the CHG film (Fig. 2 (a)) exhibited absorption bands typical of functional groups found in chitosan-glycerol films. A broad band was visible in the 3500–3200 cm^{-1} region, which corresponds to O—H and N—H stretching vibrations, as well as absorption bands at 2970–2850 cm^{-1} associated with C—H chains [46–49]. A weak absorption band centred at ca. 1650 cm^{-1} and a deeper band at 1556 cm^{-1} were also detected, related to C═O stretching vibrations (amide I band) and C—N stretching and N—H bending vibrations (amide II band) in the amide groups of chitosan [46,50,51]. The band at 1407 cm^{-1} may be related to vibrations of C–CH_3 bonds or C—O stretching in chitosan rings [49,51]. The bands at 1152 cm^{-1} and 850 cm^{-1} have previously been assigned to stretching vibrations of the C–O–C bridge, and the band centred at 1030 cm^{-1} has been associated with skeletal vibrations concerning the stretching of C—O bonds [48,50,51].

After the addition of citric acid to the chitosan-glycerol formulation (CHGCA films; Fig. 2 (a)), the most evident differences were found in the 1750–1500 cm^{-1} region. Changes in band intensity near this region have previously been associated with the cross-linking action of citric acid and the formation of new chemical bonds with glycerol, chitosan and starch [48,52–56]. A slight shift in the position of the amide II band from 1556 cm^{-1} to 1573 cm^{-1} was observed, which could be indicative of changes from primary amines to secondary amines in chitosan upon cross-linking with citric acid [48]. Additionally, a shift from ca. 1650 cm^{-1} to 1708 cm^{-1} with an increase in intensity was also detected for the amide I band, ascribed to C═O stretching vibrations. This change could be associated with ester groups between citric acid and glycerol or esterification reactions between citric acid and chitosan upon the establishment of chemical linkages between the compounds [55,56]. A new band at 1211 cm^{-1} was also formed, possibly related to C—O bonds from citric acid [57].

The FTIR spectra of the chitosan films after the addition of TPP at different concentrations (CHGCA-TPP-a, CHGCA-TPP-b and CHGCA-TPP-c; Fig. 2(a)) showed that the absorption bands became less intense, particularly those in the 3500–3200 cm^{-1} range (overlapping

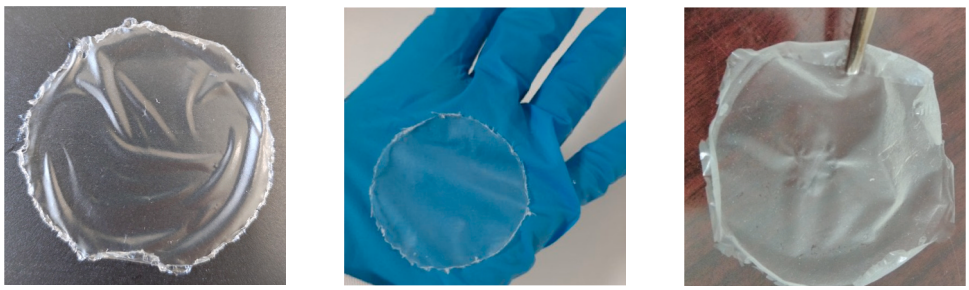

Fig. 1. CHGCA-TPP films obtained after casting the coating-forming solutions into Petri dishes and evaporating the solvent.
CHGCA-TPP: chitosan-glycerol-citric acid-sodium tripolyphosphate.

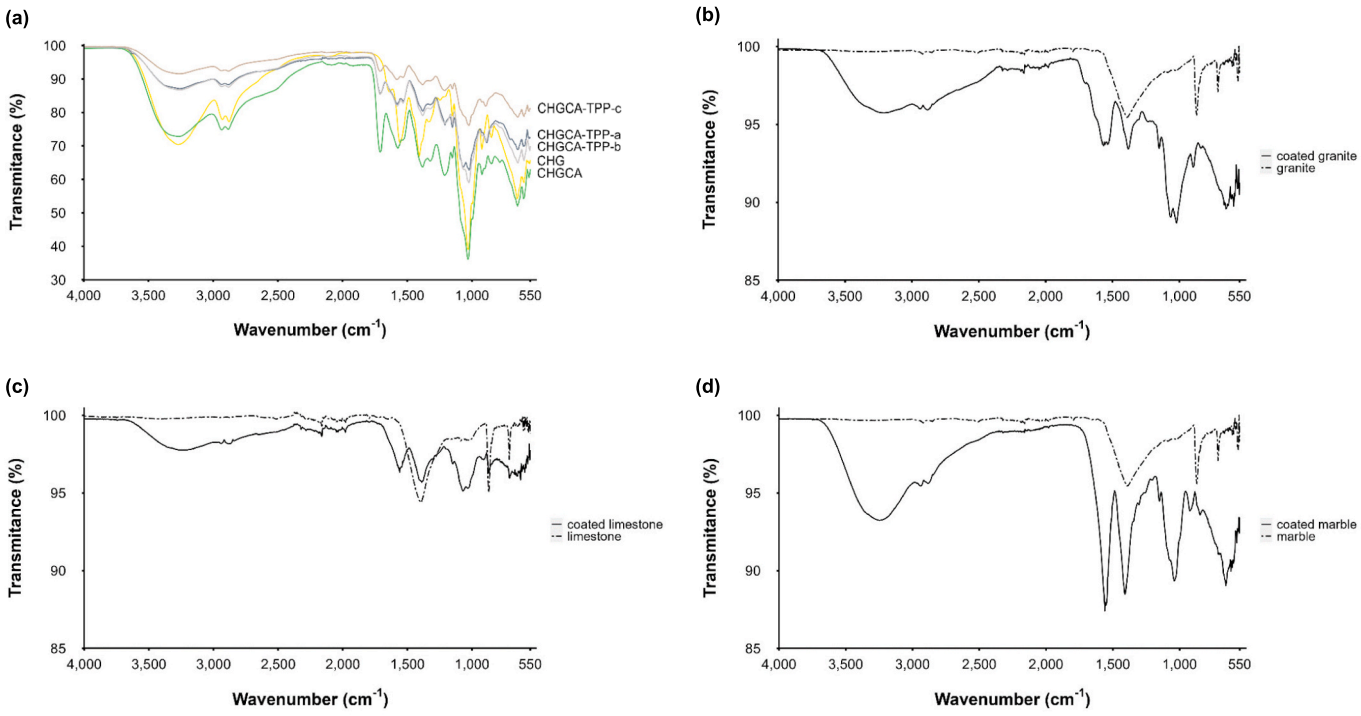

Fig. 2. FTIR spectra of (a) chitosan films and (b-d) uncoated and CHGCA-TPP-a-coated granite, limestone and marble.
CHG: chitosan-glycerol; CHGCA: chitosan-glycerol-citric acid; CHGCA-TPP: chitosan-glycerol-citric acid-sodium tripolyphosphate.

O—H and N—H vibrations), which became broader and less pronounced, possibly due to increased H-bonding upon further cross-linking by TPP [58]. Similarly, the bands at ca. 1020–1030 cm^{-1} became less intense, most clearly in the CHGCA-TPP-c film. Therefore, cross-linking reactions with citric acid and TPP were possibly indicated by slight changes in the position and intensity of the peaks rather than by the formation of new ones.

Contrary to what is reported in the literature [47,51,59], no new bands were identified in the spectra when TPP was added to the formulations, which could be related, for example, to an overlap of characteristic TPP absorption bands with those of the other compounds present in the solutions. Typical bands of TPP assigned to P═O stretching vibrations (1210 cm^{-1}), symmetric and antisymmetric stretching in PO_2 groups (1140 cm^{-1}) and symmetric and antisymmetric stretching in PO_3 groups (1093 cm^{-1}) [51,60] were presumably overlapped by absorption bands characteristic of vibrations of the C–O–C bonds of the chitosan and citric acid structures [48]. Overall, the FTIR spectra of the CHGCA-TPP films indicate that the cross-linking process of citric acid with chitosan was successfully achieved, which was further enhanced by the addition of TPP. No relevant differences among the three formulations (CHGCA-TPP-a, CHGCA-TPP-b and CHGCA-TPP-c) were observed, as strengthening of the cross-linking reactions seems to have been achieved in all samples.

3.1.2. *Film solubility and swelling in water*

The concentration of TPP significantly influenced the solubility and swelling of the films, as previously reported in other studies [59,61,62]. The solubility of the dry films after immersion in deionised water ranged from 43.64 ± 1.34 % to 55.14 ± 0.90 % and increased as a result of the higher concentration of TPP in the formulations. As illustrated in Fig. 3, increasing the chitosan:TPP mass ratio from 0.5 (CHGCA-TPP-a) to 1.5 (CHGCA-TPP-c) significantly incremented the solubility of the films ($p < 0.05$), resulting in the loss of their resistance and stability. In contrast, increasing the concentration of TPP reduced the swelling of the films. The degree of swelling decreased from 123.36 ± 17.76 % to 75.17 ± 3.18 % with increasing TPP concentrations, with CHGCA-TPP-a film exhibiting a significantly higher ($p < 0.05$) percentage of swelling than the other formulations.

Solubility and swelling in water are important factors when preparing films and coatings for application to surfaces. For stone surfaces

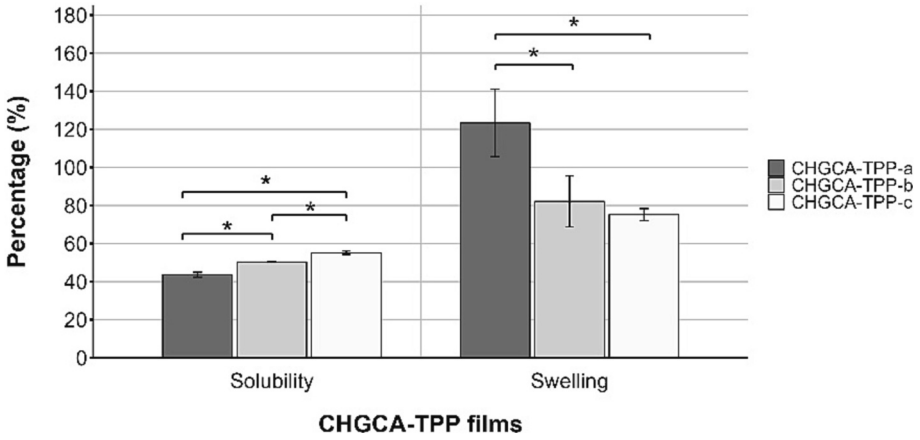

Fig. 3. – Solubility and swelling of CHGCA-TPP films.
The values shown are the mean ± SD ($n = 3$). The symbol * indicates statistically significant differences among the films (one-way ANOVA with Tukey B post-hoc test; α =0.05). CHGCA-TPP: chitosan-glycerol-citric acid-sodium tripolyphosphate.

that may come into contact with water or high humidity levels, the relative insolubility of the coatings is a requirement. Once a coating-forming solution has been applied to a surface and polymerised, the coating must retain its physical integrity and not disintegrate rapidly or expand significantly when in contact with water for a specific period of time. Therefore, in order to evaluate the solubility and swelling characteristics of the formulations, they were dried until the formation of films. The CHGCA TPP-a film, with less TPP, showed the highest percentage of swelling, suggesting it absorbed more water than the other films. This is related to groups with high affinity for water present in the film matrix, such as the amine groups in chitosan and the hydroxyl groups in chitosan and glycerol [46,63,64]. As the concentration of TPP increased, the higher degree of cross-linking in the polymer matrices may have contributed to reducing chain mobility and affinity for water, thereby limiting water influx into the matrices and lowering the degree of swelling [48,65]. The same trend was expected for the percentage of solubility. However, raising the concentration of TPP caused an increase in the solubility of the films. This may be due to the presence of more unbound polar groups that can interact with water molecules [47,61]. Nevertheless, the films mostly retained their original and intact shape at the end of the experiments, allowing for applications in programmed conservation strategies.

3.1.3. Wettability assays

The wettability assays showed that higher amounts of TPP led to smaller WCAs (Fig. 4). Statistically significant differences ($p < 0.05$) were observed only between the CHGCA-TPP-a (40.81 ± 4.45°) and CHGCA-TPP-c (31.44 ± 3.66°) films, and no differences were found when comparing these to the CHGCA-TPP-b formulation (33.84 ± 2.40°). The WCAs also decreased over time for all films (Fig. 5). Both CHGCA-TPP-a and CHGCA-TPP-b had decreases in WCAs of 11–13 % between the beginning and the end of the experiments, while CHGCA-TPP-c showed a more pronounced decrease (28 %).

The angle formed between a water droplet and the surface of a film varies according to the hydrophilicity/hydrophobicity of its constituent materials [38,66]. On the one hand, water droplets spread less over the surface of films with low wettability due to the reduced interaction between their components and the water, forming larger angles with the surfaces (> 90°) [38,66,67]. On the other hand, the interaction of water droplets with the components of films with high wettability results in greater droplet spreading and smaller contact angles (< 90°) [38,66,67]. All the films tested had WCAs <90°, revealing their high wettability and non-repellence properties, which became more evident with time as the WCA values decreased and the water droplets spread more over the surfaces of the films. Additionally, increasing amounts of TPP resulted in a decrease in WCAs and films with higher wettability, which is consistent with their higher solubility. More free polar groups could be arranged towards the surfaces of the films, making them more available to bind with water molecules [47,48]. Other studies have reached similar conclusions [61,62,68].

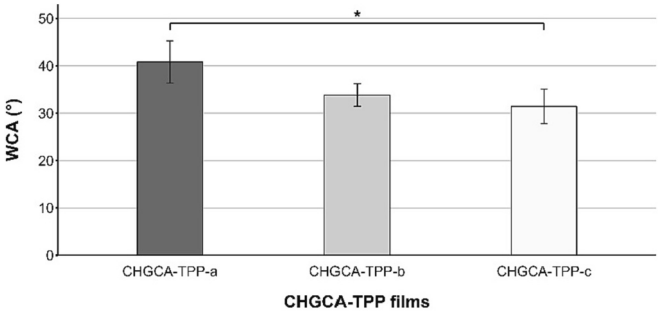

Fig. 4. Water contact angle (WCA) of CHGCA-TPP films.
The values shown are the mean ± SD ($n = 3$). The symbol * indicates statistically significant differences among the films (one-way ANOVA with Tukey B post-hoc test; α = 0.05). CHGCA-TPP: chitosan-glycerol-citric acid-sodium tripolyphosphate.

3.1.4. Film thickness and WVTR assays

The permeability of the films to water vapour was evaluated by WVTR assays (Fig. 6), which established that the CHGCA-TPP-a film was the least permeable ($p < 0.01$) with a WVTR of 140.055 ± 37.912 g m^{-2} day. Adding more TPP culminated in higher water vapour permeability, with a WVTR of 372.575 ± 14.785 g m^{-2} day recorded for CHGCA-TPP-

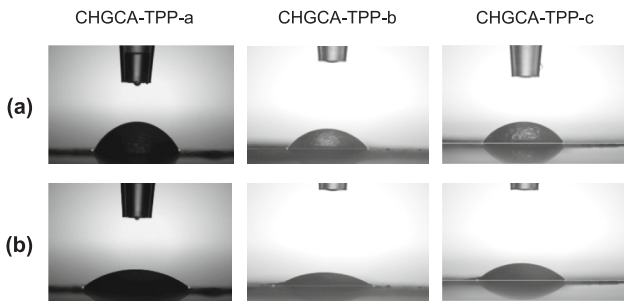

Fig. 5. Water contact angle (WCA) of CHGCA-TPP films at the (a) beginning and (b) end of the experiments, over 1 min.
CHGCA-TPP: chitosan-glycerol-citric acid-sodium tripolyphosphate.

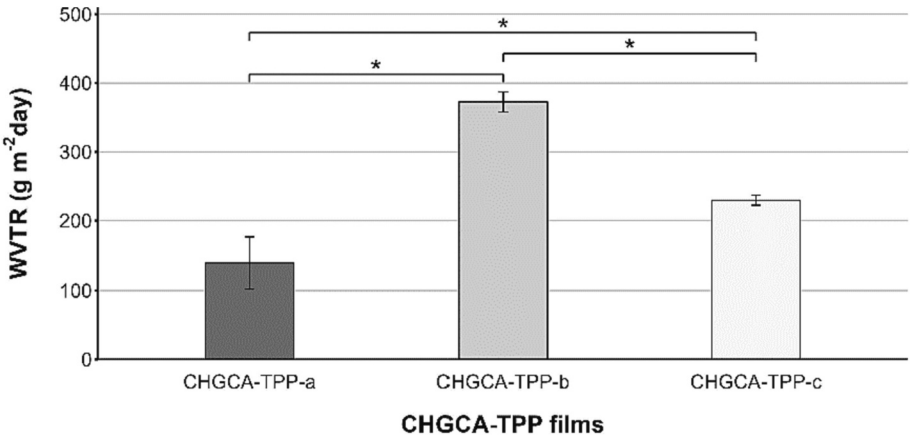

Fig. 6. – Water vapour transmission rate (WVTR) of CHGCA-TPP films.
The values shown are the mean ± SD ($n = 3$). The symbol * indicates statistically significant differences among the films (one-way ANOVA with Tukey B post-hoc test; $\alpha = 0.01$). CHGCA-TPP: chitosan-glycerol-citric acid-sodium tripolyphosphate.

b. However, when the chitosan:TPP mass ratio was further increased (CHGCA-TPP-c), the permeability decreased significantly ($p < 0.01$) and a WVTR of 229.845 ± 7.325 g m^{-2} day was obtained. The thickness (Table 1) of the films used for the permeability assays ranged from 0.040 ± 0.001 mm to 0.069 ± 0.004 mm. The CHGCA-TPP-c film was significantly thicker ($p < 0.05$) than the others, while no statistical differences were found between CHGCA-TPP-a and CHGCA-TPP-b.

Film permeability is related to empty spaces that facilitate water permeation through membranes [68]. Also, the amine and hydroxyl groups in chitosan films provide possible binding sites for water molecules, in addition to the functional groups provided by TPP that can also form bonds with water [47,61,63]. The interaction of coatings with water is important when dealing with applications for cultural heritage conservation purposes, as they must allow water vapour exchanges between the underlying surfaces and the atmosphere [19,21]. Water vapour exchanges are especially relevant for stone sculptures and artworks in outdoor settings due to the direct exposure to climatic factors, and the application of protective coatings should not cause an obstruction to water evaporation processes and water circulation in the stone pores. In this study, all chitosan-TPP films were permeable to water vapour. Increasing the concentration of TPP improved the permeability of the membranes, but only up to a certain level, beyond which a significant decrease in WVTR was observed. The increased permeability of the membranes facilitates water passage through the matrices [68]. Thus, water vapour diffusion was facilitated in the CHGCA-TPP-b film, which exhibited a significantly higher WVTR than the CHGCA-TPP-a formulation. However, the further increase in TPP concentration (CHGCA-TPP-c) may have resulted in a reduction in intermolecular distances due to the agglomeration of TPP in the polymer matrix and the formation of more compact films, thus slowing the penetration of water molecules and reducing their permeability [69,70]. This was supported by the significantly greater thickness of the CHGCA-TPP-c film.

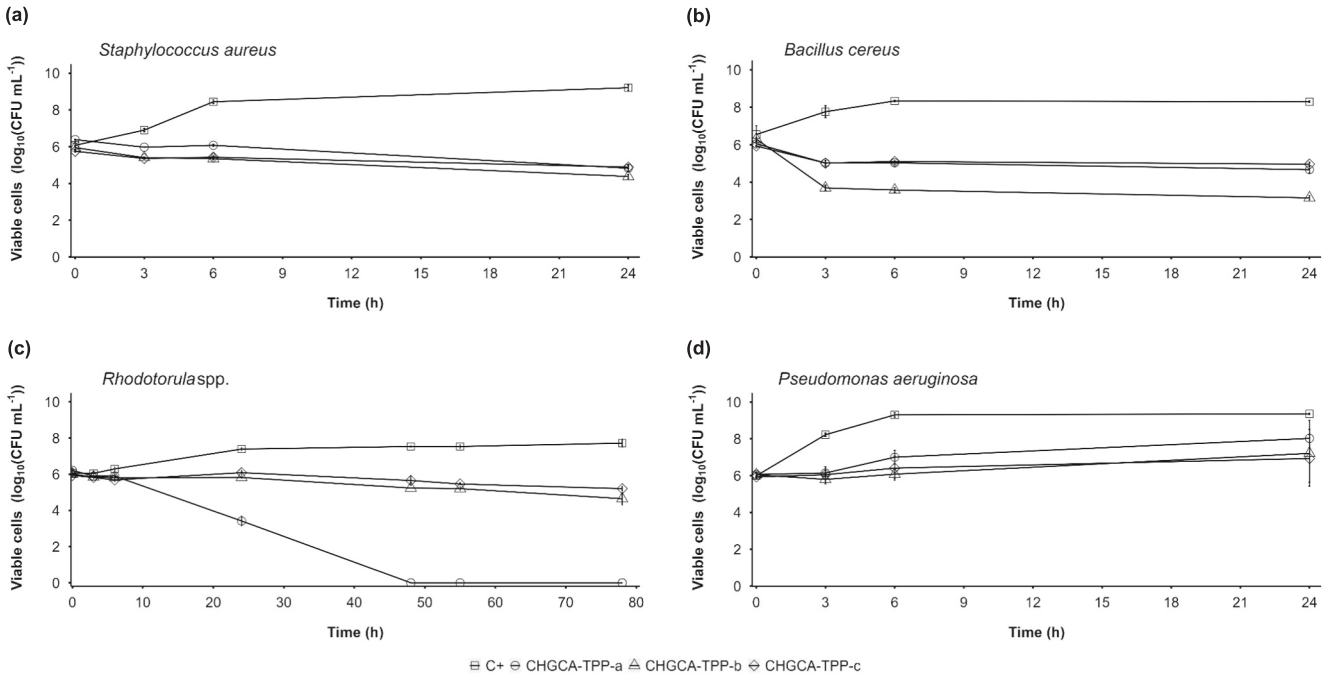

Fig. 7. Viable cell counts of (a) *Staphylococcus aureus*, (b) *Bacillus cereus*, (c) *Rhodotorula* spp. and (d) *Pseudomonas aeruginosa* incubated without chitosan films (□) or with CHGCA-TPP-a (○), CHGCA-TPP-b (△) and CHGCA-TPP-c (◇) films.

3.1.5. Antimicrobial activity

The antimicrobial properties of the films were evaluated by plotting $\log_{10}$ (CFU mL^{-1}) values over the incubation period for the Gram-positive *S. aureus* and *B. cereus*, the Gram-negative *P. aeruginosa* and the yeast *Rhodotorula* spp. (Fig. 7).

All three types of films inhibited the growth of *S. aureus*, *B. cereus* and *Rhodotorula* spp. when compared to these cell suspensions incubated without the films (positive controls). A slow and sustained decline in *S. aureus* growth was achieved over 24 h (Fig. 7 (a)), resulting in a 0.87–1.58-log reduction depending on the concentration of TPP; no statistically significant differences were found for the three formulations ($p > 0.05$).

The growth inhibition of *B. cereus* (Fig. 7 (b)) was more pronounced, with reductions of ca. 1 log cycle for the films with the highest and lowest TPP concentrations and a 3-log reduction for the film with an intermediate TPP concentration. Bacterial growth remained constant until the end of the experimental trials, with the concentration of TPP having a significant effect ($p < 0.05$) in reducing the number of viable *B. cereus* cells.

The inhibition of *Rhodotorula* spp. (Fig. 7 (c)) was noticeable after 24 h of incubation with CHGCA-TPP-a, with a reduction in its growth of ca. 3 log cycles. However, for the other two formulations only a slight decrease or no inhibition at all was achieved at this time point. The duration of the experiment was extended to 78 h to follow the exponential phase of the yeast growth, which resulted in log reduction values of 0.73 and 1.27 for those two formulations. The growth of *Rhodotorula* spp. continued to slow down steadily up to 78 h of incubation with CHGCA-TPP-a, as reflected by the almost complete absence of countable CFUs at the end of the experiment.

In contrast, incubation of *P. aeruginosa* with the films (Fig. 7 (d)) neither prevented nor substantially slowed its growth. Although the concentration of *P. aeruginosa* cells remained constant during the first 3 h, the bacterial growth resumed its typical pattern, similar to that observed in the positive control. A 2-log increase in growth was observed compared to the number of *P. aeruginosa* cells at the beginning of the experiment, and no significant differences were found among the three formulations ($p > 0.05$).

Regarding the spore concentration assays, *P. chrysogenum* colonies of ca. 21–22 mm in diameter were observed in the positive controls. All films were able to induce inhibition of *P. chrysogenum* growth (Table 1) when compared to the fungal growth on filter paper (positive control). The CHGCA-TPP-a film was the most effective inhibitor (21.48 ± 8.41 %), while those with more TPP induced inhibition rates of only 12–13 %. No significant differences were found among the films ($p > 0.05$), and only CHGCA-TPP-a showed a significantly greater inhibition than the positive control ($p < 0.05$).

The values shown are the mean ± SD ($n = 3$). CHGCA-TPP: chitosan-glycerol-citric acid-sodium tripolyphosphate.

Although it is often difficult to compare the antimicrobial activity of coatings and films across studies due to the variety of reagents and protocols employed, the antimicrobial properties of chitosan are extensively documented in the literature, against both bacterial and fungal species [46,71,72]. Citric acid has also been reported to have inhibitory effects against some bacterial strains [55]. In this study, viable cell count assays showed that all three films were effective in reducing the growth rate of *S. aureus*, *B. cereus*, *Rhodotorula* spp. and *P. chrysogenum*, although complete inhibition was only achieved for the yeast strain incubated with CHGCA-TPP-a.

The microbial inocula followed an expected pattern for the positive controls, displaying constant and increasing growth over time. However, when the same strains were incubated with the films, the concentrations of viable cells at the end of the experiments were significantly lower than at the beginning, except for *P. aeruginosa*. The lower inhibitory capacity of chitosan-based coatings against *Pseudomonas* strains compared to Gram-positive bacteria has been reported before, possibly due to the protective effect of the outer membrane of Gram-negative cells [73]. The chitosan films slowed the growth of *S. aureus* by ca. 1–1.5 orders of magnitude. However, the inhibition of bacterial growth was most evident for *B. cereus*, which showed a marked reduction in viable cell counts within just 3 h. The lower viable cell counts remained constant over time, reaching a 3-log reduction in growth after 24 h of incubation with the CHGCA-TPP-b film. These results are comparable to those obtained in a previous study in which chitosan showed bactericidal action against *B. cereus* vegetative cells within 4 h [74]. On the contrary, the CHGCA-TPP-a film produced the greatest decline in yeast growth. The number of viable *Rhodotorula* spp. cells remained close to the initial value during the first hours of the experiment, due to the typically slower growth of yeasts compared to bacteria. Nonetheless, viable yeast cell counts decreased over time and after 78 h of incubation with CHGCA-TPP-a, virtually no CFUs could be counted. This is a particularly significant result given that yeasts of the genus *Rhodotorula* are important biodeteriogens and have been associated with discolouration and visible alteration of stone monuments and mural paintings due to the production of carotenoids [41,42,75]. As for *P. chrysogenum*, although complete inhibition of the fungus was not achieved, the CHGCA-TPP-a film successfully slowed its growth compared to the positive control and produced a greater inhibition rate than the other formulations. These results are particularly noteworthy considering that the assays were performed using high concentrations of spores and their germination was still hampered when in contact with the film.

In summary, the chitosan formulations cross-linked with citric acid and TPP were successfully polymerised and exhibited partial wettability, solubility and swelling in water. However, the membranes allowed water vapour exchanges due to their high permeability. The films effectively slowed the growth of microorganisms that colonise stone heritage and contribute to its biodeterioration. However, although increasing the concentration of TPP improved some of the physicochemical properties of the coatings, the excess of TPP increased the membranes' solubility and wettability. Even though the reversibility and repeatability of conservation treatments are important, and the use of biodegradable polymers in coatings offers that possibility, high wettability/solubility of polymeric matrices is undesirable in the context of preventive conservation (especially in an outdoor setting), as it reduces their durability. For this reason, the CHGCA-TPP-a formulation was selected to test its application on stone samples, since it has a lower TPP content while retaining relevant properties.

3.2. Characterisation of CHGCA-TPP-a-coated stone samples

An overview of the characterisation procedures carried out on coated stone slabs is given in Supplementary Fig. S1.

3.2.1. Morphological assessment by scanning electron microscopy

SEM analysis (Fig. 8) revealed that the CHGCA-TPP-a solution polymerised on the surfaces of granite, limestone and marble, contrary to what was observed for the uncoated samples. However, although fragments of the coating were visible, their distribution was not uniform throughout the area of application. This uneven distribution was observed in all stone types and may be related to the natural absorption of some of the solution by the pores of the stones. Furthermore, the solution was applied and spread with a micropipette, which may also have resulted in uneven distribution on the surfaces. In situ application to a sculpture using a brush or spray may result in more uniform dispersion and polymerisation of the solution.

3.2.2. FTIR spectroscopy

The FTIR analysis of the granite, limestone and marble samples after coating with CHGCA-TPP-a confirmed that at least part of it polymerised on the stones' surfaces without being completely absorbed by their pores. This was evidenced by the FTIR spectra of the coated samples (Fig. 2 (b-d)), which were similar to the one obtained for the CHGCA-TPP-a film

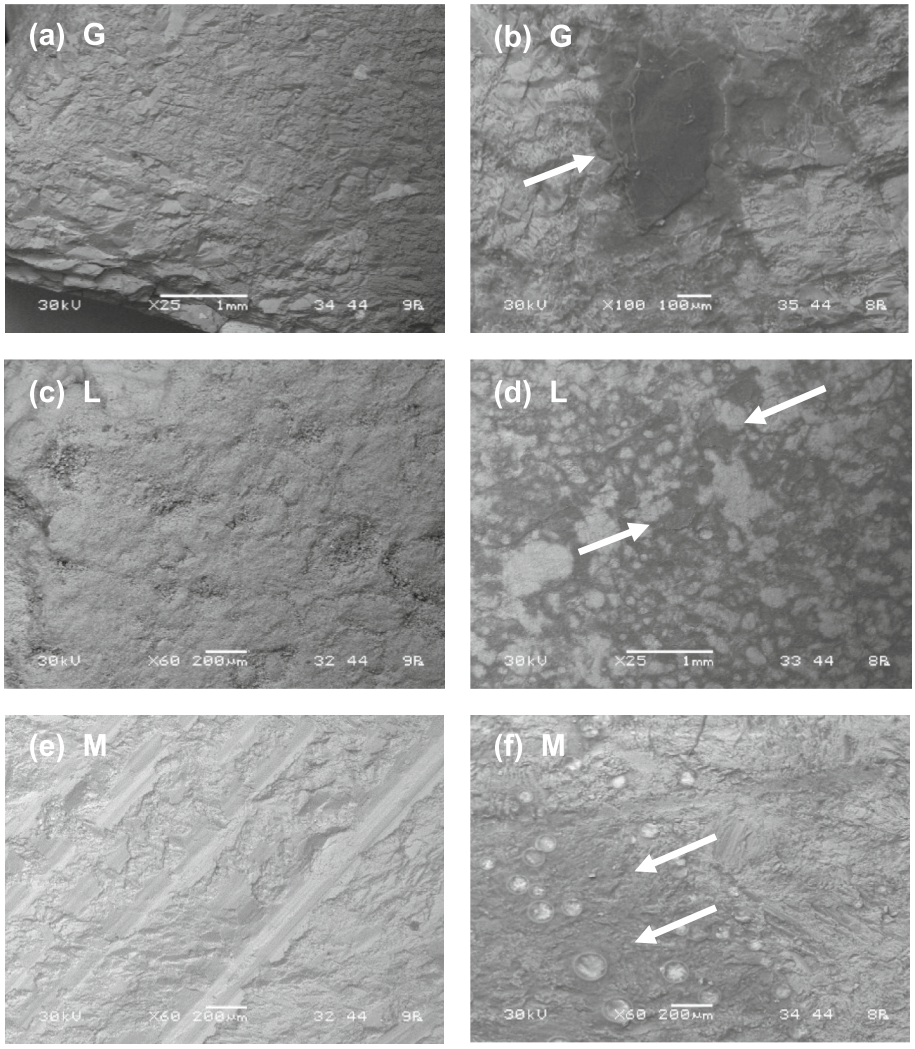

Fig. 8. Scanning electron microscopy (SEM) images of ((a), (c), (e)) uncoated and ((b), (d), (f)) CHGCA-TPP-a-coated granite, limestone and marble.
The arrows show fragments of the CHGCA-TPP-a coating. CHGCA-TPP: chitosan-glycerol-citric acid-sodium tripolyphosphate; G: granite; L: limestone; M: marble.

(Fig. 2 (a)). The main absorption bands of the functional groups identified for the CHGCA-TPP-a film were also observed on the coated stones. In particular, the broad bands in the 3500–3200 cm^{-1} and 2970–2850 cm^{-1} regions, associated with O—H, N—H and C—H bonds, were identified [46–49]. Also present were the absorption peaks at ca. 1560 cm^{-1} related to the amide II bands of chitosan, the peaks near 1400 cm^{-1} associated with vibrations in the chitosan rings, and the bands at ca. 1030 cm^{-1} related to chitosan and citric acid molecules [46,48–51]. As observed in the spectrum of the CHGCA-TPP-a film, new absorption bands pertaining to cross-linking reactions were also not visible in the spectra of the coated stones. On the contrary, the spectra of the uncoated stones did not show the distinctive bands identified for the CHGCA-TPP-a film, and only absorption peaks characteristic of the stones' mineralogical composition were visible. The spectrum of uncoated granite (Fig. 2 (b), Supplementary Fig. S2) exhibited absorption bands at 938 cm^{-1} and 761 cm^{-1}, which were within the regions assigned to Si—O asymmetric stretching in quartz and Al—O stretching in albite and biotite [76]. The spectra of limestone and marble (Fig. 2 (c) and (d), Supplementary Figs. S3 and S4) showed absorption patterns typical of calcite, with peaks at ca. 1380–1400 cm^{-1}, 870 cm^{-1} and 712 cm^{-1}, which can be attributed to the asymmetric stretching and bending modes of CO_3^{2-} [76–78].

3.2.3. *Wettability assays*

The wettability assays (Fig. 9) revealed that coating granite and limestone with the CHGCA-TPP-a solution significantly decreased the wettability of their surfaces, while not rendering them water-repellent. The WCA of coated granite (61.27 ± 4.35°) was significantly greater ($p < 0.05$) than that of the corresponding uncoated samples (29.83 ± 15.68°), as was the WCA of limestone, which was 41.94 ± 2.64° for the uncoated and 64.75 ± 4.05° for the coated samples. Therefore, the WCAs of coated granite and limestone were ca. 20° greater than that of the CHGCA-TPP-a film (see Section 3.1.3), suggesting that the coating changes the stones' intrinsic properties even though it does not act as a water-repellent.

However, this pattern was not observed for marble. The WCA of coated marble was slightly lower ($p < 0.05$) than that of its uncoated counterpart, changing from 57.18 ± 2.36° to 50.57 ± 2.06°, even though it was still within the range observed for the CHGCA-TPP-a film. The increase in wettability could be related to the morphology and porosity characteristics of the stone and its interaction with the coating. Contact angle measurements involve a very short contact time between the water droplet and the stone and are affected by surface roughness and heterogeneity [79,80]. Therefore, further studies are necessary to investigate the interaction of the coating with stone specimens.

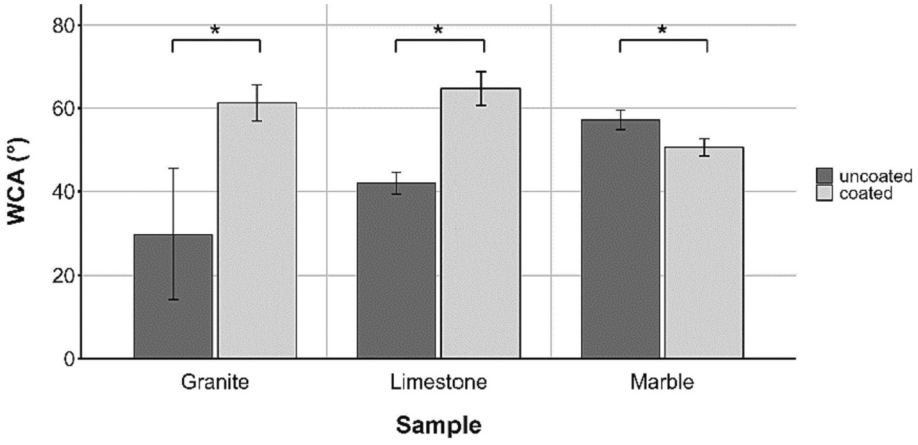

Fig. 9. Water contact angle (WCA) of uncoated and CHGCA-TPP-a-coated granite, limestone and marble.
The values shown are the mean ± SD ($n = 3$). The symbol * indicates statistically significant differences between the uncoated and coated samples (independent samples *t*-tests; $\alpha = 0.05$). CHGCA-TPP: chitosan-glycerol-citric acid-sodium tripolyphosphate.

3.2.4. *Colourimetric assays*

The colourimetric tests performed on the stones before and after the application of the coating-forming solution showed that the colour differences were small and similar between the stone types (Table 2). The colour differences when the coating was applied with a micropipette were less than or ca. 2, with the lowest value recorded for limestone. When the same coating was applied with a brush, the ΔE^*_{ab} values decreased, especially for granite and limestone, but remained similar for marble. However, no significant differences were found for any of the stone types concerning the method of coating application ($p > 0.01$).

Treatments and applications of protective coatings on art objects should not produce any perceptible aesthetic changes [81]. In cultural heritage, this assessment is commonly done using the CIELAB system to calculate the total colour difference (ΔE^*_{ab}) of many types of samples [81]. There appears to be no clear consensus in the literature regarding the acceptable limits that should be adopted for interpreting chromatic changes in stone art objects and monuments. However, some authors consider that an $\Delta E^*_{ab} < 5$ is acceptable in porous materials because any chromatic differences below this threshold cannot be detected with the naked eye [17,81–84]. Additionally, some studies suggest that $5 < \Delta E^*_{ab} < 10$ is still within a tolerable range despite already being detectable by the human eye, while an $\Delta E^*_{ab} > 10$ corresponds to visible colour changes that exceed the acceptable limit [84–86]. In this study, the ΔE^*_{ab} values were less than or equal to ca. 2, which demonstrates that coating granite, limestone and marble with the CHGCA-TPP-a solution did not cause any visible colour changes, according to the thresholds proposed in the literature cited. Moreover, the colour differences before and after the treatment remained minimal when the solution was applied with a brush to simulate a real application scenario. This supports the hypothesis that the formulation can be applied as a protective coating to these materials without causing visible colour-related aesthetic changes. However, more research on this matter is necessary to elucidate the coating-stone interactions and evaluate the establishment of a coating on the surfaces. As observed by SEM, the distribution of the formulation was not uniform, with a significant portion possibly being absorbed, which would have no effect on the colour measurements due to the absence of a protective coating at the surface level.

In summary, the CHGCA-TPP-a formulation seems to have partly polymerised on the surfaces of the stones, with a significant portion possibly absorbed into their pores. The coating decreased the wettability of granite and limestone, without making them water-repellent. Furthermore, the coating did not cause any visible colour changes, which is a prerequisite for its use as an antimicrobial protector of stone cultural heritage.

Table 2
– Total colour difference (ΔE^*_{ab}) of granite, limestone and marble coated with CHGCA-TPP-a solution using a micropipette or a brush.

Sample	ΔE^*_{ab}	
	Micropipette	Brush
Granite	2.26 ± 1.68[a]	0.97 ± 0.74[a]
Limestone	1.08 ± 0.34[a]	0.29 ± 0.11[a]
Marble	2.23 ± 0.12[a]	2.15 ± 0.27[a]

4. Conclusions

Chitosan-based formulations cross-linked with citric acid and TPP were developed with the purpose of coating stone sculptures and art objects. After polymerisation of the formulations, the resulting films were partially soluble and swelled, but the membranes were permeable to water vapour. Additionally, they were able to inhibit the growth of microorganisms that can colonise the stone and contribute to biodeterioration processes, namely the pigment-producing yeast *Rhodotorula* spp., which causes discolouration of stone substrates. However, the strains used in this study were obtained from culture collections and are a starting point for evaluating the chitosan formulations. Future studies should expand the antimicrobial activity assays in order to include a wider range of microorganisms, in particular those isolated directly from stone cultural heritage with demonstrated biodeterioration strategies. Finally, the formulation with the lowest TPP content (CHGCA-TPP-a) was applied to granite, limestone and marble while preserving their chromatic properties, and constitutes a potential antimicrobial protective coating for stone cultural heritage. Nevertheless, the stones' porosity and permeability properties should be investigated to clarify the polymerisation processes occurring when the coating is applied to lithic materials and its interaction with the substrates, as well as elucidate the coating's reticulation both at internal and surface levels and its influence on the stones' intrinsic characteristics. Likewise, the antimicrobial ability of the formulation should be confirmed after its application to different types of stone, as well as after exposure to ageing factors.

CRediT authorship contribution statement

Nádia C. Silva: Writing – review & editing, Writing – original draft, Visualization, Methodology, Investigation, Formal analysis, Data curation. **Diana Castro:** Investigation, Data curation. **Cláudia Neto:** Investigation, Data curation. **Ana Raquel Madureira:** Writing – review &

editing, Supervision, Conceptualization. **Manuela Pintado:** Writing – review & editing, Supervision, Resources, Funding acquisition, Conceptualization. **Patrícia R. Moreira:** Writing – review & editing, Supervision, Resources, Project administration, Methodology, Funding acquisition, Conceptualization.

Declaration of competing interest

The authors declare no financial or personal competing interests that are relevant to the work presented in this manuscript.

Data availability

Data will be made available on request.

Acknowledgements

The authors would like to acknowledge the financial support of this work by National Funds from FCT – Fundação para a Ciência e a Tecnologia through the project BIONANOSCULP [grant number PTDC/EPH-PAT/6281/2014], as well as the scientific collaboration under the FCT projects UID/Multi/50016/2013 and UID/Multi/50016/2019. The author Nádia C. Silva would like to thank FCT and FSE – Fundo Social Europeu for the financial support through Programa Operacional Regional Norte [grant number SFRH/BD/138935/2018], and express her gratitude to Sérgio Sousa for his assistance with SEM and to Ana Lopes for her help with the fungal growth inhibition protocol.

Appendix A. Supplementary data

Supplementary data to this article can be found online at https://doi.org/10.1016/j.porgcoat.2024.108246.

References

[1] X. Ding, W. Lan, J.-D. Gu, A review on sampling techniques and analytical methods for microbiota of cultural properties and historical architecture, Appl. Sci. 10 (2020) 8099, https://doi.org/10.3390/app10228099.
[2] S.A. Orr, J. Richards, S. Fatorić, Climate change and cultural heritage: a systematic literature review (2016–2020), Hist. Environ. Policy Pract. 12 (2021) 434–477, https://doi.org/10.1080/17567505.2021.1957264.
[3] S.E. Favero-Longo, H.A. Viles, A review of the nature, role and control of lithobionts on stone cultural heritage: weighing-up and managing biodeterioration and bioprotection, World J. Microbiol. Biotechnol. 36 (2020) 1–18, https://doi.org/10.1007/s11274-020-02878-3.
[4] G. Piñar, K. Sterflinger, Natural sciences at the service of art and cultural heritage: an interdisciplinary area in development and important challenges, Microb. Biotechnol. 14 (2021) 806–809, https://doi.org/10.1111/1751-7915.13766.
[5] P. Fernandes, Applied microbiology and biotechnology in the conservation of stone cultural heritage materials, Appl. Microbiol. Biotechnol. 73 (2006) 291–296, https://doi.org/10.1007/s00253-006-0599-8.
[6] UNESCO, Basic Texts of the 2003 Convention for the Safeguarding of the Intangible Cultural Heritage, France. https://ich.unesco.org/en/convention, 2022.
[7] UNESCO, Convention Concerning the Protection of the World Cultural and Natural Heritage. https://whc.unesco.org/en/conventiontext/, 1972.
[8] L.K. Herrera, H.A. Videla, Surface analysis and materials characterization for the study of biodeterioration and weathering effects on cultural property, Int. Biodeterior. Biodegrad. 63 (2009) 813–822, https://doi.org/10.1016/j.ibiod.2009.05.002.
[9] T.C. Dakal, S.S. Cameotra, Microbially induced deterioration of architectural heritages: routes and mechanisms involved, Environ. Sci. Eur. 24 (2012) 1–13, https://doi.org/10.1186/2190-4715-24-36.
[10] G.M. Gadd, Geomicrobiology of the built environment, Nat. Microbiol. 2 (2017) 16275, https://doi.org/10.1038/nmicrobiol.2016.275.
[11] X. Liu, R.J. Koestler, T. Warscheid, Y. Katayama, J.-D. Gu, Microbial deterioration and sustainable conservation of stone monuments and buildings, Nat. Sustain. 3 (2020) 991–1004, https://doi.org/10.1038/s41893-020-00602-5.
[12] A. Negi, I.P. Sarethy, Microbial biodeterioration of cultural heritage: events, colonization, and analyses, Microb. Ecol. 78 (2019) 1014–1029, https://doi.org/10.1007/s00248-019-01366-y.
[13] P. Tiano, Biodeterioration of stone monuments a worldwide issue, Open Conf. Proc. J. 7 (1:M3) (2016) 29–38, https://doi.org/10.2174/2210289201607020029.
[14] D. Pinna, B. Salvadori, M. Galeotti, Monitoring the performance of innovative and traditional biocides mixed with consolidants and water-repellents for the prevention of biological growth on stone, Sci. Total Environ. 423 (2012) 132–141, https://doi.org/10.1016/j.scitotenv.2012.02.012.
[15] G. Ranalli, E. Zanardini, C. Sorlini, S. Moselio, Biodeterioration-including cultural heritage, Encycl. Microbiol. (2009) 191–205, https://doi.org/10.1016/B978-012373944-5.00132-2.
[16] A. Sierra-Fernandez, L.S. Gomez-Villalba, M.E. Rabanal, R. Fort, New nanomaterials for applications in conservation and restoration of stony materials: a review, Mater. Constr. 67 (2017) e107, https://doi.org/10.3989/mc.2017.07616.
[17] S. Sasso, A.Z. Miller, M.A. Rogerio-Candelera, B. Cubero, M.L. Coutinho, L. Scrano, S.A. Bufo, Potential of natural biocides for biocontrolling phototrophic colonization on limestone, Int. Biodeterior. Biodegrad. 107 (2016) 102–110, https://doi.org/10.1016/j.ibiod.2015.11.017.
[18] S. Di Salvo, Nanotechnology for cultural heritage, Int. J. Sci. Technol. Soc. 2 (2014) 28, https://doi.org/10.11648/j.ijsts.20140202.12.
[19] Z. Kaplan, H. Böke, A. Sofuoglu, B. İpekoğlu, Long term stability of biodegradable polymers on building limestone, Prog. Org. Coat. 131 (2019) 378–388, https://doi.org/10.1016/j.porgcoat.2019.03.004.
[20] F. Sbardella, M.P. Bracciale, M.L. Santarelli, J.M. Asua, Waterborne modified-silica/acrylates hybrid nanocomposites as surface protective coatings for stone monuments, Prog. Org. Coat. 149 (2020) 105897, https://doi.org/10.1016/j.porgcoat.2020.105897.
[21] G. Giuntoli, L. Rosi, M. Frediani, B. Sacchi, P. Frediani, Fluoro-functionalized PLA polymers as potential water-repellent coating materials for protection of stone, J. Appl. Polym. Sci. 125 (2012) 3125–3133, https://doi.org/10.1002/app.36469.
[22] B. Appelbaum, Criteria for treatment: reversibility, J. Am. Inst. Conserv. 26 (1987) 65–73, https://doi.org/10.1179/019713687806027852.
[23] M. Favaro, R. Mendichi, F. Ossola, U. Russo, S. Simon, P. Tomasin, P.A. Vigato, Evaluation of polymers for conservation treatments of outdoor exposed stone monuments. Part I: photo-oxidative weathering, Polym. Degrad. Stab. 91 (2006) 3083–3096, https://doi.org/10.1016/j.polymdegradstab.2006.08.012.
[24] S. Andreotti, E. Franzoni, M.D. Esposti, P. Fabbri, Poly(hydroxyalkanoate)s-based hydrophobic coatings for the protection of stone in cultural heritage, Materials (Basel) 11 (2018) 165, https://doi.org/10.3390/ma11010165.
[25] Y. Ocak, A. Sofuoglu, F. Tihminlioglu, H. Böke, Protection of marble surfaces by using biodegradable polymers as coating agent, Prog. Org. Coat. 66 (2009) 213–220, https://doi.org/10.1016/j.porgcoat.2009.07.007.
[26] S.M. Ahsan, M. Thomas, K.K. Reddy, S.G. Sooraparaju, A. Asthana, I. Bhatnagar, Chitosan as biomaterial in drug delivery and tissue engineering, Int. J. Biol. Macromol. 110 (2018) 97–109, https://doi.org/10.1016/j.ijbiomac.2017.08.140.
[27] S. Chaudhary, S. Kumar, V. Kumar, R. Sharma, Chitosan nanoemulsions as advanced edible coatings for fruits and vegetables: composition, fabrication and developments in last decade, Int. J. Biol. Macromol. 152 (2020) 154–170, https://doi.org/10.1016/j.ijbiomac.2020.02.276.
[28] G. Kerch, Chitosan films and coatings prevent losses of fresh fruit nutritional quality: a review, Trends Food Sci. Technol. 46 (2015) 159–166, https://doi.org/10.1016/j.tifs.2015.10.010.
[29] P.S. Bakshi, D. Selvakumar, K. Kadirvelu, N.S. Kumar, Chitosan as an environment friendly biomaterial – a review on recent modifications and applications, Int. J. Biol. Macromol. 150 (2020) 1072–1083, https://doi.org/10.1016/j.ijbiomac.2019.10.113.
[30] Z. Shariatinia, Pharmaceutical applications of chitosan, Adv. Colloid Interf. Sci. 263 (2019) 131–194, https://doi.org/10.1016/j.cis.2018.11.008.
[31] R.V. Kumaraswamy, S. Kumari, R.C. Choudhary, A. Pal, R. Raliya, P. Biswas, V. Saharan, Engineered chitosan based nanomaterials: bioactivities, mechanisms and perspectives in plant protection and growth, Int. J. Biol. Macromol. 113 (2018) 494–506, https://doi.org/10.1016/j.ijbiomac.2018.02.130.
[32] G.M. Mathew, D.C. Mathew, R.K. Sukumaran, R. Sindhu, C.-C. Huang, P. Binod, R. Sirohi, S.-H. Kim, A. Pandey, Sustainable and eco-friendly strategies for shrimp shell valorization, Environ. Pollut. 267 (2020) 115656, https://doi.org/10.1016/j.envpol.2020.115656.
[33] M. Rinaudo, Chitin and chitosan: properties and applications, Prog. Polym. Sci. 31 (2006) 603–632, https://doi.org/10.1016/j.progpolymsci.2006.06.001.
[34] S. Kumar, A. Mukherjee, J. Dutta, Chitosan based nanocomposite films and coatings: emerging antimicrobial food packaging alternatives, Trends Food Sci. Technol. 97 (2020) 196–209, https://doi.org/10.1016/j.tifs.2020.01.002.
[35] H. Haghighi, F. Licciardello, P. Fava, H.W. Siesler, A. Pulvirenti, Recent advances on chitosan-based films for sustainable food packaging applications, Food Packag. Shelf Life 26 (2020) 100551, https://doi.org/10.1016/j.fpsl.2020.100551.
[36] N. Sawtarie, Y. Cai, Y. Lapitsky, Preparation of chitosan/tripolyphosphate nanoparticles with highly tunable size and low polydispersity, Colloids Surf. B: Biointerfaces 157 (2017) 110–117, https://doi.org/10.1016/j.colsurfb.2017.05.055.
[37] Z. Cui, E.S. Beach, P.T. Anastas, Modification of chitosan films with environmentally benign reagents for increased water resistance, Green Chem. Lett. Rev. 4 (2011) 35–40, https://doi.org/10.1080/17518253.2010.500621.
[38] L. Al-Naamani, S. Dobretsov, J. Dutta, Chitosan-zinc oxide nanoparticle composite coating for active food packaging applications, Innov. Food Sci. Emerg. Technol. 38 (2016) 231–237, https://doi.org/10.1016/j.ifset.2016.10.010.
[39] S. Scheerer, O. Ortega-Morales, C. Gaylarde, Microbial deterioration of stone monuments - an updated overview, in: A.I. Laskin, S. Sariaslani, G.M. Gadd (Eds.), Adv. Appl. Microbiol., 1st editio, Academic Press, 2009: pp. 97–139. doi: https://doi.org/10.1016/S0065-2164(08)00805-8.
[40] Q. Li, B. Zhang, X. Yang, Q. Ge, Deterioration-associated microbiome of stone monuments: structure, variation, and assembly, Appl. Environ. Microbiol. 84 (2018), https://doi.org/10.1128/AEM.02680-17 e02680-17.

[41] A.C. Pinheiro, N. Mesquita, J. Trovão, F. Soares, I. Tiago, C. Coelho, H. Paiva de Carvalho, F. Gil, L. Catarino, G. Piñar, A. Portugal, Limestone biodeterioration: a review on the Portuguese cultural heritage scenario, J. Cult. Herit. 36 (2019) 275–285, https://doi.org/10.1016/j.culher.2018.07.008.
[42] T. Rosado, A. Reis, J. Mirão, A. Candeias, P. Vandenabeele, A.T. Caldeira, Pink! Why not? On the unusual colour of Évora cathedral, Int. Biodeterior. Biodegrad. 94 (2014) 121–127, https://doi.org/10.1016/j.ibiod.2014.07.010.
[43] D. Campos, C. Piccirillo, R.C. Pullar, P.M.L. Castro, M.M.E. Pintado, Characterization and antimicrobial properties of food packaging methylcellulose films containing stem extract of Ginja cherry, J. Sci. Food Agric. 94 (2014) 2097–2103, https://doi.org/10.1002/jsfa.6530.
[44] A. Guimarães, Ó. Ramos, M. Cerqueira, A. Venâncio, L. Abrunhosa, Active whey protein edible films and coatings incorporating lactobacillus buchneri for Penicillium nordicum control in cheese, Food Bioprocess Technol. 13 (2020) 1074–1086, https://doi.org/10.1007/s11947-020-02465-2.
[45] A.I. Lopes, A. Melo, C. Caleja, E. Pereira, T.C. Finimundy, T.B. Afonso, S. Silva, M. Ivanov, M. Sokovi, F.K. Tavaria, L. Barros, M. Pintado, Evaluation of antimicrobial and antioxidant activities of alginate edible coatings incorporated with plant extracts, Coatings 13 (2023) 1487, https://doi.org/10.3390/coatings13091487.
[46] A. Pavinatto, A.V. de A. Mattos, A.C.G. Malpass, M.H. Okura, D.T. Balogh, R. C. Sanfelice, Coating with chitosan-based edible films for mechanical/biological protection of strawberries, Int. J. Biol. Macromol. 151 (2020) 1004–1011, https://doi.org/10.1016/j.ijbiomac.2019.11.076.
[47] M. Gierszewska, J. Ostrowska-Czubenko, Chitosan-based membranes with different ionic crosslinking density for pharmaceutical and industrial applications, Carbohydr. Polym. 153 (2016) 501–511, https://doi.org/10.1016/j.carbpol.2016.07.126.
[48] P. Guerrero, A. Muxika, I. Zarandona, K. de la Caba, Crosslinking of chitosan films processed by compression molding, Carbohydr. Polym. 206 (2019) 820–826, https://doi.org/10.1016/j.carbpol.2018.11.064.
[49] M. Bagheri, H. Younesi, S. Hajati, S.M. Borghei, Application of chitosan-citric acid nanoparticles for removal of chromium (VI), Int. J. Biol. Macromol. 80 (2015) 431–444, https://doi.org/10.1016/j.ijbiomac.2015.07.022.
[50] Y. Liu, X. Shen, H. Zhou, Y. Wang, L. Deng, Chemical modification of chitosan film via surface grafting of citric acid molecular to promote the biomineralization, Appl. Surf. Sci. 370 (2016) 270–278, https://doi.org/10.1016/j.apsusc.2016.02.124.
[51] P. Sacco, M. Borgogna, A. Travan, E. Marsich, S. Paoletti, F. Asaro, M. Grassi, I. Donati, Polysaccharide-based networks from homogeneous chitosan-tripolyphosphate hydrogels: synthesis and characterization, Biomacromolecules 15 (2014) 3396–3405, https://doi.org/10.1021/bm500909n.
[52] F. Garavand, M. Rouhi, S.H. Razavi, I. Cacciotti, R. Mohammadi, Improving the integrity of natural biopolymer films used in food packaging by crosslinking approach: a review, Int. J. Biol. Macromol. 104 (2017) 687–707, https://doi.org/10.1016/j.ijbiomac.2017.06.093.
[53] N. Reddy, Y. Yang, Citric acid cross-linking of starch films, Food Chem. 118 (2010) 702–711, https://doi.org/10.1016/j.foodchem.2009.05.050.
[54] X. Ma, P.R. Chang, J. Yu, M. Stumborg, Properties of biodegradable citric acid-modified granular starch/thermoplastic pea starch composites, Carbohydr. Polym. 75 (2009) 1–8, https://doi.org/10.1016/j.carbpol.2008.05.020.
[55] H. Wu, Y. Lei, J. Lu, R. Zhu, D. Xiao, C. Jiao, R. Xia, Z. Zhang, G. Shen, Y. Liu, S. Li, M. Li, Effect of citric acid induced crosslinking on the structure and properties of potato starch/chitosan composite films, Food Hydrocoll. 97 (2019) 105208, https://doi.org/10.1016/j.foodhyd.2019.105208.
[56] P.G. Seligraa, C.M. Jaramillob, L. Famáa, S. Goyanesa, Biodegradable and non-retrogradable eco-films based on starch – glycerol with citric acid as crosslinking agent, Carbohydr. Polym. 138 (2016) 66–74, https://doi.org/10.1016/j.carbpol.2015.11.041.
[57] N. Sharmin, J.T. Rosnes, L. Prabhu, U. Böcker, M. Sivertsvik, Effect of citric acid cross linking on the mechanical, rheological and barrier properties of chitosan, Molecules 27 (2022) 5118, https://doi.org/10.3390/molecules27165118.
[58] M.R. de Moura, F.A. Aouada, R.J. Avena-Bustillos, T.H. McHugh, J.M. Krochta, L. H.C. Mattoso, Improved barrier and mechanical properties of novel hydroxypropyl methylcellulose edible films with chitosan/tripolyphosphate nanoparticles, J. Food Eng. 92 (2009) 448–453, https://doi.org/10.1016/j.jfoodeng.2008.12.015.
[59] A.F. Tomaz, S.M.S. de Carvalho, R.C. Barbosa, S.M.L. Silva, M.A.S. Gutierrez, A.G. B. de Lima, M.V.L. Fook, Ionically crosslinked chitosan membranes used as drug carriers for cancer therapy application, Materials (Basel) 11 (2018) 2051, https://doi.org/10.3390/ma11102051.
[60] F. Mi, H. Sung, S. Shyu, C. Su, C. Peng, Synthesis and characterization of biodegradable TPP/genipin co- crosslinked chitosan gel beads, Polymer (Guildf) 44 (2003) 6521–6530, https://doi.org/10.1016/S0032-3861(03)00620-7.
[61] C. Wu, J. Sun, Y. Lu, T. Wu, J. Pang, Y. Hu, In situ self-assembly chitosan/ε-polylysine bionanocomposite film with enhanced antimicrobial properties for food packaging, Int. J. Biol. Macromol. 132 (2019) 385–392, https://doi.org/10.1016/j.ijbiomac.2019.03.133.
[62] R.A. Lusiana, W.P. Protoningtyas, A.R. Wijaya, D. Siswanta, S.J. Santosa Mudasir, Chitosan-tripoly phosphate (CS-TPP) synthesis through cross-linking process: the effect of concentration towards membrane mechanical characteristic and urea permeation, Orient. J. Chem. 33 (2017) 2913–2919, https://doi.org/10.13005/ojc/330626.
[63] M. Mujtaba, A.M. Salaberria, M.A. Andres, M. Kaya, A. Gunyakti, J. Labidi, Utilization of flax (Linum usitatissimum) cellulose nanocrystals as reinforcing material for chitosan films, Int. J. Biol. Macromol. 104 (2017) 944–952, https://doi.org/10.1016/j.ijbiomac.2017.06.127.
[64] R. Priyadarshi, B. Sauraj, Y.S. Kumar, Negi, chitosan film incorporated with citric acid and glycerol as an active packaging material for extension of green chilli shelf life, Carbohydr. Polym. 195 (2018) 329–338, https://doi.org/10.1016/j.carbpol.2018.04.089.
[65] T.T. Nguyen, U.T. Thi Dao, Q.P. Thi Bui, G.L. Bach, C.N. Ha Thuc, H. Ha Thuc, Enhanced antimicrobial activities and physiochemical properties of edible film based on chitosan incorporated with Sonneratia caseolaris (L.), Engl. leaf extract, Prog. Org. Coatings. 140 (2020) 105487, https://doi.org/10.1016/j.porgcoat.2019.105487.
[66] M.A.V. Rodrigues, M.R.V. Bertolo, C.A. Marangon, C.A. Martins, A.M. de G. Plepis, Chitosan and gelatin materials incorporated with phenolic extracts of grape seed and jabuticaba peel: rheological, physicochemical, antioxidant, antimicrobial and barrier properties, Int. J. Biol. Macromol. 160 (2020) 769–779, https://doi.org/10.1016/j.ijbiomac.2020.05.240.
[67] K.-Y. Law, Definitions for hydrophilicity, hydrophobicity, and superhydrophobicity: getting the basics right, J. Phys. Chem. Lett. 5 (2014) 686–688, https://doi.org/10.1021/jz402762h.
[68] R.A. Lusiana, V.D.A. Sangkota, N.A. Sasongko, G. Gunawan, A.R. Wijaya, S. J. Santosa, D. Siswanta, M. Mudasir, M.N.Z. Abidin, S. Mansur, M.H.D. Othman, Permeability improvement of polyethersulfone-polietylene glycol (PEG-PES) flat sheet type membranes by tripolyphosphate-crosslinked chitosan (TPP-CS) coating, Int. J. Biol. Macromol. 152 (2020) 633–644, https://doi.org/10.1016/j.ijbiomac.2020.02.290.
[69] I.K. Sani, S. Pirsa, Ş. Tağı, Preparation of chitosan/zinc oxide/Melissa officinalis essential oil nano-composite film and evaluation of physical, mechanical and antimicrobial properties by response surface method, Polym. Test. 79 (2019), https://doi.org/10.1016/j.polymertesting.2019.106004.
[70] E. Sogut, H. Cakmak, Utilization of carrot (Daucus carota L.) fiber as a filler for chitosan based films, Food Hydrocoll. 106 (2020) 105861, https://doi.org/10.1016/j.foodhyd.2020.105861.
[71] D.R. Perinelli, L. Fagioli, R. Campana, J.K.W. Lam, W. Baffone, G.F. Palmieri, L. Casettari, G. Bonacucina, Chitosan-based nanosystems and their exploited antimicrobial activity, Eur. J. Pharm. Sci. 117 (2018) 8–20, https://doi.org/10.1016/j.ejps.2018.01.046.
[72] R.C. Goy, D. De Britto, O.B.G. Assis, A review of the antimicrobial activity of chitosan, Polim. Ciência e Tecnol. 19 (2009) 241–247, https://doi.org/10.1590/S0104-14282009000300013.
[73] V. Coma, A. Deschamps, A. Martial-Gros, Bioactive packaging materials from edible chitosan polymer - antimicrobial activity assessment on dairy-related contaminants, J. Food Sci. 68 (2003) 2788–2792, https://doi.org/10.1111/j.1365-2621.2003.tb05806.x.
[74] J.C. Fernandes, P. Eaton, A.M. Gomes, M.E. Pintado, F. Xavier Malcata, Study of the antibacterial effects of chitosans on Bacillus cereus (and its spores) by atomic force microscopy imaging and nanoindentation, Ultramicroscopy 109 (2009) 854–860, https://doi.org/10.1016/j.ultramic.2009.03.015.
[75] N.C. Silva, A.R. Madureira, M. Pintado, P.R. Moreira, Biocontamination and diversity of epilithic bacteria and fungi colonising outdoor stone and mortar sculptures, Appl. Microbiol. Biotechnol. 106 (2022) 3811–3828, https://doi.org/10.1007/s00253-022-11957-4.
[76] O. Rudic, J. Ranogajec, T. Vulic, S. Vucetic, D. Cjepa, D. Lazar, Photo-induced properties of TiO2/ZnAl layered double hydroxide coating onto porous mineral substrates, Ceram. Int. 40 (2014) 9445–9455, https://doi.org/10.1016/j.ceramint.2014.02.017.
[77] M.K. Khallaf, A.A. El-Midany, S.E. El-Mofty, Influence of acrylic coatings on the interfacial, physical, and mechanical properties of stone-based monuments, Prog. Org. Coat. 72 (2011) 592–598, https://doi.org/10.1016/j.porgcoat.2011.06.021.
[78] A. Sdiri, T. Higashi, T. Hatta, F. Jamoussi, N. Tase, Mineralogical and spectroscopic characterization, and potential environmental use of limestone from the Abiod formation, Tunisia, environ, Earth Sci. 61 (2010) 1275–1287, https://doi.org/10.1007/s12665-010-0450-5.
[79] D. Colangiuli, M. Lettieri, M. Masieri, A. Calia, Field study in an urban environment of simultaneous self-cleaning and hydrophobic nanosized TiO2-based coatings on stone for the protection of building surface, Sci. Total Environ. 650 (2019) 2919–2930, https://doi.org/10.1016/j.scitotenv.2018.10.044.
[80] M. Lettieri, D. Colangiuli, M. Masieri, A. Calia, Field performances of nanosized TiO2 coated limestone for a self-cleaning building surface in an urban environment, Build. Environ. 147 (2019) 506–516, https://doi.org/10.1016/j.buildenv.2018.10.037.
[81] J. Becerra, M. Mateo, P. Ortiz, G. Nicolás, A.P. Zaderenko, Evaluation of the applicability of nano-biocide treatments on limestones used in cultural heritage, J. Cult. Herit. 38 (2019) 126–135, https://doi.org/10.1016/j.culher.2019.02.010.
[82] M. Tortora, M. Chiarini, N. Spreti, C. Casieri, 1H-NMR-relaxation and colorimetry for evaluating nanopolymeric dispersions as stone protective coatings, J. Cult. Herit. 44 (2020) 204–210, https://doi.org/10.1016/j.culher.2019.12.014.
[83] G.B. Goffredo, S. Accoroni, C. Totti, T. Romagnoli, L. Valentini, P. Munafò, Titanium dioxide based nanotreatments to inhibit microalgal fouling on building stone surfaces, Build. Environ. 112 (2017) 209–222, https://doi.org/10.1016/j.buildenv.2016.11.034.

[84] M. Lettieri, M. Masieri, Surface characterization and effectiveness evaluation of anti-graffiti coatings on highly porous stone materials, Appl. Surf. Sci. 288 (2014) 466–477, https://doi.org/10.1016/j.apsusc.2013.10.056.
[85] O. García, K. Malaga, Definition of the procedure to determine the suitability and durability of an anti-graffiti product for application on cultural heritage porous materials, J. Cult. Herit. 13 (2012) 77–82, https://doi.org/10.1016/j.culher.2011.07.004.
[86] P. Ortiz, V. Antúnez, R. Ortiz, J.M. Martín, M.A. Gómez, A.R. Hortal, B. Martínez-Haya, Comparative study of pulsed laser cleaning applied to weathered marble surfaces, Appl. Surf. Sci. 283 (2013) 193–201, https://doi.org/10.1016/j.apsusc.2013.06.081.